Impact of Fe^0 amendment on methylene blue discoloration by sand columns

Miyajima K.[a], Noubactep C.[a,b,*]

[a]Angewandte Geologie, Universität Göttingen, Goldschmidtstraße 3, D-37077, Göttingen, Germany.

[b]Kultur und Nachhaltige Entwicklung CDD e.V., Postfach 1502, D-37005 Göttingen, Germany

* corresponding author: e-mail: cnoubac@gwdg.de; Tel. +49 551 39 3191, Fax: +49 551 399379.

Abstract

The influence of metallic iron (Fe^0) amendment on the efficiency of sand to discolor a 2.0 mg L^{-1} methylene blue (MB) solution was investigated in column studies. MB was used as an indicator to identify the optimum Fe^0/sand ratio for efficient filtration systems. Columns contained 0, 100 or 200 g of a Fe^0 material. The volumetric proportion of Fe^0 in the reactive layer of the columns with 100 g of material varied from 10 to 100 %. Results showed that, Fe^0 amendment significantly impaired MB discoloration by sand for experiments lasting for up to 132 days. Early MB breakthrough in Fe^0/sand columns delineated the paramount importance of particle cementation, which has caused preferential flow with a negative impact on discoloration efficiency. The most efficient Fe^0/sand mixtures were the ones with 30 to 50 % Fe^0 (v/v). These volumetric ratios correspond 33 to 41 % weight ratios showing that the commonly used 1:1 weight ratio (50 %) may not be optimal. Further research with compounds exhibiting different affinities to both Fe^0 and sand is needed before this observation can be generalized.

Keywords: Fe^0/sand filters, Particle cementation, Permeability loss, Water treatment, Zero-valent iron.

1 Introduction

Metallic iron (Fe^0) has been demonstrated in numerous studies to represent one of the best available materials for subsurface permeable reactive barriers [1-6]. Fe^0 is also a very efficient material for above-ground wastewater treatment and safe dinking water provision [7-9]. New

applications of Fe^0 for water treatment usually involve extensive pilot-scale studies although several models have been developed for predicting the performance of Fe^0 material [10-13]. Moreover, despite 20 years of intensive research, the question as to whether iron should be used alone or mixed to a cost efficient material is yet to be properly addressed [14-24].

The suitability of Fe^0 for water treatment arises from its aqueous instability (Eq. 1 - 4). Immersed Fe^0 is oxidized by water according to Eq. 1:

$$Fe^0 + 2\ H^+ \Rightarrow Fe^{2+} + H_2\uparrow \quad (1)$$

$$Fe^0 + ½\ O_2 + H_2O \Rightarrow Fe^{2+} + 2\ HO^- \quad (2)$$

$$2\ Fe^{2+} + ½\ O_2 + H_2O \Rightarrow 2\ Fe^{3+} + 2\ HO^- \quad (3)$$

$$Fe^{n+} + n\ HO^- \Rightarrow Fe(OH)_n \quad \Rightarrow FeOOH/Fe_xO_y \quad (4)$$

In the presence of dissolved O_2 the more favourable redox reaction is given by Eq. 2, but reaction following Eq. 1 still significantly occurs due to the abundance of water [25]. Moreover, it has been traceably shown that even under external oxic conditions, Fe^0 is oxidized by water (Eq. 1) and Fe^{II} by O_2 (Eq. 3) [26]. In other words, accelerated Fe^0 oxidation under oxic conditions results from Fe^{II} consumption by O_2 (Le Chatelier's principle) and not from any direct interactions between Fe^0 and O_2 [26,27].

The sustainability of Fe^0 filtration systems primarily depends on the intrinsic reactivity of Fe^0 which oxidative dissolution induces both contaminant removal [28] and porosity loss due to the volumetric expansive nature of iron corrosion [29]. Aqueous iron oxidation yields hydroxides (e.g. $Fe(OH)_2$) and oxides (e.g. Fe_3O_4) (Eq. 4) which volume varies from 2.1 to 6.4 times the volume of Fe^0 in the metal [30]. The transformation of Fe^0 to (hydr)oxides (Eqs. 1 through 4) goes through colloidal intermediates with cementing capacities. Here, cementation means that the inter-granular space is filled by Fe^{II}/Fe^{III} precipitates and the solid particles are "cemented" to each other. This cementation results in material consolidation and in permeability loss in column experiments [14,16,31]. The ease with which cementation is observed primarily depends also on the reaction environments (oxic vs. anoxic). However, the

first tool to restrict cementation is to decrease the proportion of cement producers, that is to mix Fe^0 with a non expansive material (e.g. activated carbon, anthracite, clay, gravel, organic substances, pumice, sand) [32].

The literature contains many contradictory findings regarding the question as to whether admixing inert materials to micro-scale Fe^0 is beneficial for its performance or not [17,20,24,33]. Inert materials have been routinely mixed with Fe^0 to (i) avoid/delay/minimize Fe^0 cementation [14-16], (ii) increase the hydraulic conductivity [1,15,19] and (iii) decrease the cost of the barrier [18]. Recent theoretical works have demonstrated that admixing non expansive materials (e.g. gravel, MnO_2, pumice, sand, TiO_2) to Fe^0 is a pre-requisite for sustainable Fe^0 filtration systems [34].

The present work is the first attempt to experimentally test the validity of the concept that admixing non expansive materials to Fe^0 is a pre-requisite for sustainable (e.g. long-term efficient) Fe^0 filtration systems. For this purpose, the discoloration of aqueous methylene blue (MB) is investigated in ten columns containing 0 g (1 column), 100 g (8 columns) or 200 g (1 column) of a commercial Fe^0. The tested Fe^0/sand volumetric ratios were 0/100, 10/90, 20/80, 30/70, 40/60, 50/50, 70/30, 80/20 and 100/0. Individual systems are characterized by the time-dependent evolution of (i) the extent of iron release, (ii) the MB breakthrough and (iii) the hydraulic conductivity.

2 Background of the experimental methodology

The choice of methylene blue (MB) as model pollutant to ascertain the optimal Fe^0/sand ratio for sustainable efficient Fe^0-based filters arises from three major factors: (i) the ease of MB determination by cost-efficiency colorimetric methods, (ii) the low affinity of MB to iron oxides (corrosion products) [35], and the high affinity of MB to sand [36,37]. The low affinity of MB for iron corrosion products suggests that the retention time of MB in a Fe^0-based system will be minimal (rapid breakthrough). The breakthrough time is further lowered by working under atmospheric conditions (oxic conditions) where voluminous corrosion

products are generated [30,38]. Despite low affinity to iron oxides, MB is removed in Fe^0-based filters mainly by adsorptive size-exclusion. However, adsorption and co-precipitation still occur [39], but their extent depends on the flow velocity or the residence time of the solution within the filter.

The suitability of Fe^0-amended sand filters to investigate the impact of the corrosion process on the efficiency (MB discoloration, permeability loss) of a sand filter (reference system) arises from the historical observation by Mitchell et al. [35], that sand is a better adsorbing agent for MB than iron oxide coated sand. In other words, the discoloration performance of a Fe^0-amended sand filter is worsen by the progressive coating of sand by in-situ generated iron oxides (assumption 1). On the other hand, the accumulation of corrosion products in a system will reduce the porosity and lower its hydraulic conductivity (assumption 2).

The used methodology for the investigation of the impact of the Fe^0/sand ratio on the efficiency investigated system comprises testing the validity of assumption 1 and assumption 2 by following the extent of (i) MB discoloration and (ii) permeability loss in Fe^0-ammended sand columns.

3 Materials and methods

3.1 Solutions

3.1.1 Methylene blue (MB)

MB is widely used as model contaminant to characterize the suitability of various materials for water treatment [35-37, 40-42]. The used methylene blue (MB) was of analytical grade. The working solution has a concentration of 2.0 mgL^{-1} and was weekly prepared by diluting a 1000 mg L^{-1} stock solution using the tap water of the city of Göttingen. Its average composition (in mg L^{-1}) was: Cl^-: 12.9; NO_3^-: 7.5; SO_4^{2-}: 35.5; Na^+: 9.7; K^+: 0.9; Mg^{2+}: 8.2; Ca^{2+}: 37.3. The pH value of the initial solution was 8.2. The used concentration 2.0 mg L^{-1} or 6.3 μM was selected to approach the concentration range of natural waters (MB as model micro-pollutant).

3.1.2 Iron

A standard iron solution (1000 mg L^{-1}) from Baker JT® was used to calibrate the spectrophotometer used for analysis. All other chemicals used were of analytical grade. In preparation for spectrophotometric analysis, ascorbic acid was used to reduce Fe^{III} in solution to Fe^{II}. 1,10 orthophenanthroline (ACROS Organics) was used as reagent for Fe^{II} complexation. Other chemicals used in this study included L(+)-ascorbic acid and L-ascorbic acid sodium salt.

3.2 Solid materials

3.2.1 Metallic iron (Fe^0)

The used Fe^0 material was purchased from iPutech (Rheinfelden, Germany). The material is available as fillings with a particle size between 0.3 and 2.0 mm. Its elemental composition as specified by the supplier was: C: 3.52%; Si: 2.12%; Mn: 0.93%; Cr: 0.66%. The material was used without any further pre-treatment. Fe^0 was proven a powerful discoloration agent for MB with the particularity, that discoloration agents are progressively generated in-situ [39]. Therefore, the discoloration capacity of used Fe^0 can not be exhausted within the experimental duration (here 132 days).

3.2.2 Sand

The used sand was a commercial material for aviculture (“Papagaiensand” from RUT – Lehrte/Germany). Papagaiensand was used as received without any further pre-treatment or characterization. The particle size was between 0.5 and 2.0 mm. Sand was used as an MB adsorbent [35] because of its worldwide availability and its use as admixing agent in Fe^0/H_2O systems [1,24,34]. The adsorption capacity of sand for MB can be exhausted within the experimental duration.

3.3 MB discoloration

As-received Fe^0 from iPutec GmbH (Rheinfelden, Germany) was used. The materials were packed into columns in a dual manner. Sand ($H_{sand,1}$ and $H_{sand,2}$ – Tab. 1) and pure Fe^0 layers

(columns 9 and 10 – Tab. 1) were wet packed. For all other reactive zones (< 100 % Fe^0), dry homogenized Fe^0/sand mixtures were introduced into the column in small lofts, which were wetted and compacted with manual tapping. To warrant optimal compaction, columns were gently tapped with a 100 mL PET flacon containing water. Tested volumetric ratios of Fe^0 in the reactive zone (Tab. 1) were built while using the volume occupied by 100 g of Fe^0 (32 mL – apparent volume) as unity. The resulting sand masses are documented in Tab. 1. For example, the system with 20 % (v/v) Fe^0, was made up of one volume of Fe^0 and four volumes of sand. The corresponding mass of sand was 77 g yielding a weight ratio of 43.5 %.

The 2.0 mg L^{-1} MB solution was pumped upwards from PE bottles using a peristaltic pump (Ismatec, ICP 24). Tygon tubes were used to connect inlet reservoir, pump, column and outlet. Ten glass columns (40 cm long, 2.6 cm inner diameter) having a section of 5.31 cm^2 were used. The columns were mostly packed with sand (Tab. 1, Fig. 1). The extent of MB discoloration by packed materials and the extent of the permeability loss by individual column set-ups (Tab. 1) were the sole targets. The experiments were performed at room temperature (22 ± 3 °C). A stable flow rate of 0.1 mL min^{-1} was maintained throughout the experiment.

The whole effluent was collected. The volume recorded as function of the elapsed time served for the assessment of flow velocity or hydraulic conductivity. Each collected fraction was analysed for MB and dissolved Fe.

3.4 Analytical methods

MB and aqueous iron concentrations were determined by a Cary 50 UV-Vis spectrophotometer (Varian) at a wavelength of 664.5 nm and 510 nm respectively. Cuvettes with 1 cm light path were used. The iron determination followed the 1,10 orthophenanthroline method [43]. The spectrophotometer was calibrated for MB concentrations ≤ 2.5 mg L^{-1} and iron concentrations ≤ 10.0 mg L^{-1}. The pH value was measured by combined glass electrodes (WTW Co., Germany).

3.5 Presentation of experimental results

158 The MB breakthrough curves are expressed in terms of normalized concentration defined as
159 the ratio of effluent dye concentration to inlet dye concentration (C/C_0) as a function of time
160 or volume of effluent for a given bed height. For each column set-up, the extent of MB
161 discoloration (efficiency, E in %) at each time was calculated according to the following
162 equation (Eq. 5):

163 $$E = [(\Sigma V_i * C_0 - \Sigma V_i * C_i)/\Sigma V_i * C_0] * 100\% \quad (5)$$

164 where C_0 is the initial aqueous MB concentration (2.0 mg L^{-1}), while C_i gives the MB
165 concentration in each collected sample V_i.
166 In order to characterize the effect of the tested column set-ups on MB discoloration at the end
167 of the experiment, the discoloration efficiency (E) and the specific discoloration (E_s) were
168 calculated using Eq. 6 and Eq. 7.

169 $$E = m_{discol}/m_{in} * 100 \quad (6)$$

170 $$E_s = m_{discol}/m_{Fe} * 100 \quad (7)$$

171 where m_{in} is the mass of MB flowed into the column, m_{discol} is the MB mass discoloured
172 within the reactive zone, and m_{Fe} the mass of Fe^0 present in the column. It is operationally
173 assumed that $H_{sand,2}$ (Tab. 1) does not significantly impact MB discoloration if significant
174 flow disturbance happens in the reactive zone (assumption 3). The extent of MB discoloration
175 (m_{MB} in mg) within the reactive zone of individual columns was calculated from $H_{sand,1}$ using
176 the rule of proportion. In this effort, column 1 was used as reference (44 cm of sand for 48.78
177 mg MB) (Eq. 8). 48.78 mg is the value of m_{discol} ($m_{discol} = \Sigma V_i * C_0$) at MB breakthrough in the
178 pure sand column.

179 $$m_{MB}\ (mg) = (H_{sand,1}/44) * 48.78 \quad (8)$$

180 **4 Results and Discussion**

181 **4.1 Visual analysis of the columns at day 132**

182 Figure 1 reveals 4 main colorations: blue, brown, dark-green and ‘white’. White is the
183 operational colour of sand as seen in the upper part of columns 9 and 10, blue is the colour of

adsorbed methylene blue (column 1), brown is the product of Fe^0 oxidation by dissolved O_2, and dark-green is the colour of Fe^{II} species (including green rust). The formation of rust (brown coloration) is the most tangible evidence of corrosion by O_2. That is either the local iron oxidation by O_2 or the migration of Fe^{III} species (e.g. $Fe(OH)_3$, $Fe_2O_3 \bullet H_2O$). In other words, a brown coloration 'far' from the entrance zone of the reactive layer is an evidence of O_2 breakthrough.

It is important to notice that MB breakthrough is observed in all systems although an homogeneous blue coloration is only see in system 1 (0 % Fe^0) and in the lower part of all other columns ($H_{sand,1}$ – Tab. 1). This observation indicates that flow disturbance was caused within the Fe^0-containing layer. In other words, uniform flow may be limited to pure sand layers (column 1, H_{sand1}).

In general, from the inlet to the outlet, Fe^0-containing columns exhibited the following coloration sequence: (i) blue ($H_{sand,1}$), (ii) brown (entrance of the reactive layer), (iii) grey or dark (reactive layer), (iv) dark-green (entrance of $H_{sand,2}$) and (v) white ($H_{sand,2}$). Columns 7 and 8 exhibited a different behaviour as the entrance zone of the $H_{sand,2}$ layer was brown coloured (not green-dark). This coloration indicates that dissolved O_2 could be quantitatively transported across the reactive layer in these 2 systems. Additionally, a blue coloration is seen in the upper part of column 7.

The presence of a brown coloration in the connecting tube at the column outlet for all Fe^0-containing systems shows that there is an axial breakthrough of O_2 as a rule. In other words, the O_2 breakthrough is the first hint for preferential flow due to particle cementation. The second hint for preferential flow is the blue coloration in upper sand layer of column 7. The absence of the brown coloration in the upper sand layer of systems with less than 70 % Fe^0 is concordant with the use of Fe^0/sand mixtures as 'O_2 scavengers' [2,3,14].

4.2 Evidence for an optimal system with less than 70 % Fe^0

Table 2 summarizes the results from the 10 columns. It shows that about 38.0 L of the MB solution flow through each column during the 132 days. This corresponds to about 69 mg of MB (effective initial concentration 1.83 mg L^{-1}) from which 42.0 to 63.3 % was discoloured within the reactive layer in Fe^0-containing systems (columns 2 to 10). On the other hand, dissolved iron release from the same columns (4.0 to 47.1 mg) represented only less than 0.05 % of the initial Fe^0 amount (100 or 200 g).

An important result from Tab. 2 is that the reference system (0 % Fe^0 – column 1) was the most efficient system with 72.3 % MB discoloration efficiency at the day 132 (E value - Fig. 2). Therefore, assumption 1 is validated. However, at this date the discoloration capacity of this system is almost exhausted because this is a pure adsorption system [44,45]. In column 1 (97 % breakthrough), 48.79 mg MB is adsorbed onto 360 g of sand, yielding an adsorption capacity of 0.138 mg g^{-1}. For Fe^0-containing system, not such adsorption capacity can be defined because MB is not adsorbed onto a defined surface, rather MB is adsorbed or enmeshed in the matrix of iron corrosion products [46]. Additionally, the extent of Fe^0 depletion is difficult to access.

Figure 2 summarizes the results of the evolution of the specific MB discoloration (E_s in μg g^{-1}) as a function of the volumetric proportion of Fe^0 in the reactive zone. It is seen that E_s evolutes through a maximum at 30 % Fe^0. E_s then decreases to a minimum at 80 % Fe^0. The overall trend that, for long enough experimental durations, contaminant removal should be minimal (i) in the sand column (pure adsorbent with limited capacity) and (ii) in pure Fe^0 column (no room for expansive iron corrosion) is found here. The fact that the pure Fe^0 system (100 % Fe^0) is more efficient than the 80 % Fe^0 system is due to the simplistic nature of assumption 3 (no MB discoloration in $H_{sand,2}$) as attested by the blue coloration in the $H_{sand,2}$ layer in column 7 (Fig. 1). MB discoloration is normalized to 360 g of sand in the reference system and to (only) 100 g Fe^0 in all other systems. This is the reason for the apparent discrepancy between E and E_s values in Fig. 2.

The most important output from Fig. 2 is that for the same mass of Fe^0, various E_s values (143 to 239 μg g^{-1}) are obtained after 132 days. These results clearly question the suitability/validity of E_s as indicator of Fe^0 efficiency when experimental conditions are not identical/similar. Fe^0 is definitively not an adsorbent but a generator of 'MB scavengers'. Accordingly, the discoloration efficiency/capacity of Fe^0 for MB can not be universally defined. Therefore, results from Fig. 2 radically refute the generalized use of 'removal capacity' as indicator of the efficiency of Fe^0 materials.

4.3 Iron breakthrough

Figure 3 summarizes the results of the evolution of dissolved iron concentration in the effluent (also see Tab. 2). It is seen that Fe release and migration occurs in three stages: (i) dissolution from Fe^0, (ii) short distance migration due to the low solubility at pH > 5, and (iii) adsorption and precipitation on sand particle (in situ coating). This in situ coating is responsible for the accelerated MB breakthrough because of porosity loss and lower adsorptive affinity [35]. Fig. 3 shows that the largest iron release (up to 8.0 mg L^{-1}) was observed in the system with the lowest Fe^0 volumetric proportion of Fe^0 (10 %). This column corresponds to the system with $H_{sand,2}$ = 0. The next system (30 % Fe^0) exhibiting noticeable iron breakthrough (> 2 mg L^{-1}) hast the lowest $H_{sand,2}$-value (11 cm). This observation confirms the fact, that the long-distance transport of dissolved iron is not favoured at pH > 5 [47]. In all other systems, even more iron could have been dissolved but it is retained within the reactive layer and the under laying sand ($H_{sand,2}$ > 11 cm) (dark-green coloration – section 3.1). The retention mechanisms are (i) adsorption onto available iron oxides or onto sand, or (ii) precipitation as iron (hydr)oxides. It is very important to notice that the extent of iron release depends primarily on the intrinsic reactivity of used Fe^0. Although data on iron release from column experiments are available in the literature [15] it is quite impossible to make a quantitative comparison. In fact, a parameter (or an index) to characterize the intrinsic reactivity of Fe^0 is still lacking [48].

The fact that in situ dissolved iron mostly remains in the system is a hint, that MB should be more or less quantitatively removed by adsorption, co-precipitation and adsorptive size exclusion (straining) [46]. As recalled in section 3.2, all Fe^0/sand systems should be more efficient that pure sand system (assumption 4). Testing the validity of assumption 4 will sustain the further presentation.

4.4 Behaviour of the columns

Fig. 4 (a and b) and Tab. 3 summarize the results of the 10 columns (see also Tab. 2). Figure 4 depicts the time-dependant evolution of the MB mass in the effluent. It can be seen that breakthrough occurs after at least 18 mg of MB was retained in all systems. This corresponds to complete discoloration of 9.0 L of the initial solution.

Fig. 4b shows that the reference system (0 % Fe^0) is the most efficient at discoloring MB for the tested experimental duration (132 days). This observation seemingly disproves assumption 4. However, it should be recalled that the adsorption capacity of sand is limited. Therefore, it can be argued that 'early breakthrough' in Fe^0-amended systems is due to the low reactivity of used Fe^0 as it could not produce enough 'scavengers' for MB removal (assumption 5).

The system with 80 % Fe^0 was the less efficient (Tab. 2). The remaining systems could be ordered as follows: 70 % < 100 % < 10 % < 20 % < 50 % < 40 % < 30 %. Since sand is a good adsorbent for MB, the classification has to take the thickness of sand preceding the reactive layer into account ($H_{sand,1}$ - see sections 3.2 and 3.5). However, the absence of a monotone trend in the evolution of the systems disproves assumption 5. Therefore, another process, yet to be identified is responsible for the 'early breakthrough' of MB in Fe^0-amended systems.

Fig. 4b compares the efficiency of the reference system (0 % Fe^0) with that of pure Fe^0 systems (column 9 and 10 – Tab. 1). The sand-column remains the most efficient but the column with 200 g Fe^0 was more efficient than the column with 100 g Fe^0. This is a further evidence that Fe^0 disturbs the efficiency of sand for MB discoloration but not in a monotone

linear way. While further disproving assumption 5 (but validating assumption 1), this observation suggest that a stochastic process is responsible for the 'early breakthrough' of MB in systems with 100 g Fe^0 (assumption 6).

Fig. 4 also shows that after breakthrough the mass MB (mg) in the effluent linearly increases. The regression parameters (a and b values) of the lines $[MB]_{effluent} = a*[MB]_{influent} + b$ were determined with Origin 6.0 and summarized in Tab. 3. The slope of this line can be regarded as the rate of MB increase in the effluent after breakthrough. For a pure absorbent the 'a value' ideally approaches zero corresponding to a S-shape breakthrough. In other words, the smaller the 'a value', the more the system is close to an adsorbing system. The classification of the systems after the order of increasing 'a values' is: 0 % < 30 % < 40 % < 50 % < 20 % < 10 % < 75 % = 100 % < 80 %. It is interesting that both columns with 100 % Fe^0 (100 and 200 g) exhibited the same a value (0.65). This fact is an important hint that despite differences in the thickness the same 'stochastic processes' are responsible for MB discoloration. The difference between both 100 % Fe^0-columns is the 'b value': -14.6 for 100 g and -23.0 for 200 g. Here again, the absence of a simple proportion between the two 'b values' is a hint of the stochastic nature of processes occurring in Fe^0/H_2O systems and leading to 'early breakthrough' relative to the pure sand system (0 % Fe^0).

4.5 Effect of the thickness $H_{sand,1}$

Fig. 1 showed that the reference system (first column from left) was entirely blue colored while in all other systems, the uniform blue color is limited to the sand before the Fe^0 layer or reactive zone ($H_{sand,1}$ - Tab. 1). This observation suggests that, in Fe^0-containing systems, granular particles (Fe^0 and sand) are partly cemented and preferential flow is generated in the Fe^0 layer.

If it is mentally assumed that the Fe^0 layer depicted no interactions with MB, the solution would have 'traversed' the Fe^0 layer non-disturbed and the uniform blue coloration would have continued after the pure Fe^0 (columns 9 and 10) or the Fe^0-amended layer (columns 2 to

8). However, as reported by Imamura et al. [49] MB adsorbs strongly onto Fe^0 materials. Therefore, the absence of a uniform blue coloration can be attributed to the flow disturbance in the Fe^0 layer (assumption 2 is validated). Additionally, Mitchell et al. [35] have traceably demonstrated that iron oxide-coated sand is a poorer adsorbent for MB than pure sand. It is the objective of this study to characterize the processes occurring within the reactive layer. The initial Fe^0 dissolution creates a local super-saturation of aqueous Fe which is short-term diffusive transported and precipitated as cement, in particular the observed brown coloration at the entrance of the reactive layer. Particle cementation is certainly a stochastic process, suggesting that assumption 6 may be valid.

Fig. 5 summarized the results of a mathematical modelling of the time to breakthrough in the Fe^0-amended columns. The time necessary for 0.5 breakthrough in the pure sand column (day 97) is used as reference. The model used Eq. 8 while replacing the mass by the time where $C/C_0 = 0.5$ in column 1 (96.83 days - Eq. 9). In the case "sand1 & 2", "$H_{sand,1}$" is replaced by "$H_{sand,1} + H_{sand,2}$" (Tab. 1).

$$t_{BT}\ (\text{days}) = (H_{sand,1}/44) * 96.83 \qquad (9)$$

As a rule, the longer the time to breakthrough, the more efficient a system. Fig. 5 shows that the most efficient systems were the systems with 30, 40 and 50 vol % Fe^0. It is seen that the observed efficiency is always higher than the efficiency of H_{sand1}, while for $Fe^0 > 40$ % the efficiency of the system was lesser than that of sand alone ('sand 1 & 2'). This observation corroborates the complexity of processes in the Fe^0-ammended and pure Fe^0 layers. It should be kept in mind that the data presented in Fig. 5 ('observed' in particular) are static snap-shots of dynamic processes (time for 0.5 MB breakthrough in the sand column). However, they clearly show that systems with Fe^0 volumetric ratios ≥ 70 % are less efficient than systems containing 30 to 50 vol % Fe^0.

4.6 Hydraulic conductivity

The results presented in Fig. 6 clearly demonstrate that the hydraulic conductivity almost remained constant during the whole experiment. This unusual observation could be misinterpreted as the absence of porosity loss due to expansive iron corrosion. However, the used material is known for its reactivity and the observed brown coloration (section 3.1) attests that oxidative dissolution and subsequent precipitation of iron hydroxides has occurred. One should keep in mind, that permeability loss is observed whenever the sum of forces generated in the system (filter resistance) are superior to the pressure supplied by the peristaltic pump (initial driving force) (Eq. 10).

$$\text{Flow rate} = \text{Driving force} / \text{Filter resistance} \quad (10)$$

In the present work, it could be concluded that the used pump flow rate (0.1 mL min^{-1}) was sufficient to transport enough in situ generated iron oxides out of the reactive zone and so to avoid significant clogging (for 132 days). Fig. 1b shows that, in all Fe^0-based systems, colloidal Fe species have escaped from the columns and precipitated in the connection tubes.

Figure 7 schematically shows the time-dependent evolution of the porosity in a Fe^0/sand cylindrical column while Fe^0 experiences uniform corrosion. It is seem that porosity loss should increase with the experimental duration (assumption 2). This trend was not observed in the current study (Fig 6). This observation is rationalized by the fact that the filter resistance generated by 100 or 200 g of Fe^0 for up to 132 days was not sufficient to significantly induce a decrease of the flow rate (hydraulic conductivity). However, material compaction was observed and its thickness was smaller in systems with higher Fe^0 proportions (Tab. 2). Accordingly, although no significant permeability loss is noticed, particle cementation has impacted the uniform flow in various extent in individual columns. Assumption 2 is thus validated.

The driving force (hydraulic pressure) from Eq. 10 is ideally uniformly distributed in the whole column. That is on all Fe^0 and sand particle within the 44 cm effective length. However, due to the cementation process described above, there are local ‘irregularities’, as

364 cemented particles are non accessible and cemented regions non/less permeable. For example,
365 Eq. 10 suggests that if a 50 % porosity loss occurs ($t_{1/2}$ in Fig. 7), the hydraulic pressure
366 should be doubled to maintain the observed constant flow. Actually, a local increase of the
367 hydraulic pressure has occurred and has caused preferential flow at a certain distance from the
368 'clogged zone'. This accelerated flow is illustrated the best by the brown colour in the $H_{sand,2}$
369 layer as observed in columns 7 and 8 (Fig. 1, section 3.1).
370 The fact that column 7 and 8 depicted the lowest Es efficiency (Fig. 2) is a further
371 confirmation of assumption 4 ("all Fe^0/sand systems should be more efficient that pure sand
372 system") as the observed anomaly results from the particular difficulty to uniformly mix Fe^0
373 and sand when Fe^0 is in volumetric abundance. It should be recalled that sound theoretical
374 works [50] have proven the needlessness of testing these volumetric proportions. Therefore, it
375 is not worth to continue the discussion on these systems. Accordingly, further research should
376 focus on Fe^0 ratios < 60 % while eventually test the pure Fe^0 as negative reference.
377 **4.7 MB breakthrough**
378 Figure 8 summarizes the results of MB breakthrough. A S-shaped breakthrough curve was
379 obtained for all systems but only the reference system experienced a complete breakthrough
380 (C/C_0 = 0.97 at day 132).
381 The breakthrough time (time for [MB] ≠ 0) varied largely and was primarily dependent on the
382 thickness of $H_{sand.1}$. As shown in Fig. 8a, individual columns depicted slightly different
383 behaviour but the discoloration efficiency was levelled at about C/C_0 = 0.70. This levelling at
384 C/C_0 = 0.70 suggests that the 'residual' (steady state) corrosion rate was sufficient to induce
385 the discoloration of about 30 % of a 2.0 mg L^{-1} MB. In other words, an effluent solution
386 containing about 0.60 mg L^{-1} MB (30 % of 2 mg L^{-1}) could be efficiently treated (no MB
387 breakthrough) for the 132 days of the experiment. As a rule, natural waters contain much
388 lower levels of contaminants termed 'micro-pollutants' [51]. Remember that the experiments
389 were designed to characterize the efficiency of Fe^0 at various Fe^0/sand ratios using limited

390 amounts of Fe^0. Accordingly, both MB breakthrough and the characterization of the system
391 thereafter were intended.
392 Fig. 8b summarized the MB breakthrough behaviour in the 3 pure material systems (100 %
393 sand or Fe^0). Its shows that the sand systems is the most efficient for 132 days but that the
394 breakthrough is quantitative (100 %) suggested that the adsorption capacity is exhausted.
395 From this moment on, no significant MB discoloration is expected. On the contrary, in the
396 pure Fe^0 systems the initial S-shape breakthrough starting after 25 and 50 days respectively is
397 levelled at about 70 % (C/C_0 = 0.70). Fig. 8b reveals that after a short levelling at 70 %
398 breakthrough, 'additional removal' occurred in the system with 200 g Fe^0 followed by a phase
399 of limited removal efficiency. This 'fluctuation' is also be evident from Fig. 8a, in particular
400 for the 30 % Fe^0 system. These 'fluctuations' document the uncertainty in the long-term
401 reactivity of Fe^0 materials. This observation supports the quest to accumulate data on long-
402 term reactivity of various Fe^0 materials at laboratory scale [48].
403 The breakthrough results suggest the efficient use of Fe^0/sand systems in beds for water
404 treatment in deep filtration modus. However, design efforts are urgently needed. It is observed
405 from Fig. 8a that the time to achieve breakthrough is the highest for systems containing 30 to
406 50 % Fe^0 (v/v).

407 **4.8 Discussion**

408 **4.8.1 Validating the used experimental methodology**

409 The presentation herein is centred on testing the validity of two fundamental (1,2) and four
410 operational (3-6) assumptions. Assumptions 1 through 6 are summarized and commented in
411 this section.

Assumption 1: the (initial) MB discoloration performance of a Fe^0-amended sand filter is worsen by the progressive coating of sand by in-situ generated iron oxides. Assumption 1 is verified by experimental data for up to 132 days, clearly showing that the sand system (reference system) is the most efficient for MB discoloration.

Assumption 2: the accumulation of corrosion products in a system reduces its porosity and lowers the hydraulic conductivity (permeability loss). Assumption 2 is indirectly verified as the used pump flow rate (0.1 mL min^{-1}) was sufficient to avoid accumulation of corrosion products in columns containing only 100 g of Fe^0 during 132 days. It is recommended that lower pump flow rates are tested in future works. Alternatively, higher Fe^0 amounts (> 100 g) may be tested using the pump flow rate of 0.1 mL min^{-1}.

Assumption 3: the sand layer after the Fe^0 layer ($H_{sand,2}$ - Tab. 1) does not significantly impact MB discoloration if significant flow disturbance happens in the reactive zone. This assumption was not verified showing the complexity of processes coupled to Fe^0 amendment of sand filters.

Assumption 4: All Fe^0/sand systems are more efficient than the pure sand system. This assumption was disproved by experimental data for up to 132 days. However, the fact that the MB removal capacity of the reference system (sand only) was almost exhausted at day 132 suggests that this assumption could be valid for longer experimental durations if the systems are not clogged. Exactly this was the goal of the present study: identifying the optimal Fe^0/sand ratio concealing increased permeability (more sand) and decreased efficiency (more sand or less Fe^0). It is essential to point out, that MB presents all the characteristics of a tracer [52,53]. In particular, its very low affinity to the Fe^0/H_2O system makes it an ideal compound to characterize the impact of iron corrosion on the hydraulic properties of a Fe^0 amended filter.

Assumption 5: the 'early' MB breakthrough in Fe^0-amended systems is due to the low reactivity of used Fe^0 as it could not produce enough 'scavengers' for MB removal. This

assumption was disproved an corroborates the 'tracer nature' of MB for characterizing the process of iron corrosion in packed-bed filtration systems. In essence, produced iron oxides either accelerated MB breakthrough.

Assumption 6: a stochastic (non linear) process is responsible for the 'early' MB breakthrough in Fe^0-amended systems. Assumption 6 was validated by experimental data. This validation seriously questions the current approach of correlating Fe^0 reactivity with monitored parameters at the system outlet including the extent of H_2 evolution and the extent of contaminant removal [22-24].

The validation of the two fundamental assumptions (1 and 2) is regarded as the validation of the theory of Fe^0-based filtration systems presented in ref. [34]. This makes the assertion that pure Fe^0 systems (100 % Fe^0) are not sustainable universal. This was even already experimentally observed as Fe^0 systems used for As removal in South East Asia (Bangladesh, Nepal) were very efficient but not sustainable [7]. With respect of the longed optimal Fe^0/sand ratio, the present work could identify the domain in which it should be sought: 30 to 50 % Fe^0 (v/v).

4.8.2 Significance of achieved results

The present study was designed to characterize the behaviour of Fe^0 columns at discolouring MB when the 100 g Fe^0 represents a volumetric proportion varying from 10 to 100 %. Using identical columns, the same initial flow rate (multi-channel peristaltic pump) and the same sand as an additive material, initial differences include the thickness of the reactive layer (H_{rz}) and the thickness of sand after the reactive layer ($H_{sand,2}$). To better discuss the impact of the thickness of sand after the reactive layer on the extend of Fe release from the column, the thickness of sand before the reactive layer ($H_{sand,1}$) was also varied (Tab. 1).

Figure 9 summarizes the results of the cumulative MB discoloration (Eq. 5) as function of $H_{sand,1}$, H_{rz} and $H_{sand,2}$. It is evident that from each system, the E value decreases with increasing experimental duration. For example, the 0 % Fe^0 system ($H_{sand,1}$ = 44 cm; H_{rz} =

464 $H_{sand,2}$ = 0 cm) exhibits E values of 100.0, 89.5 and 72.3 % for 55, 77 and 132 days
465 respectively.
466 Fig. 9 shows a rough trend that (i) E values increase with increasing $H_{sand,1}$ value; (ii) there is
467 an optimum H_{rz} value of around 10 - 15 cm, (ii) no trend is observed for the $H_{sand,2}$ values.
468 The optimum in the H_{rz} (11 to 15 cm) curve coincides with the results discussed in 3.5
469 showing that 30 to 50 % Fe^0 is the optimal range for efficient systems. This coincidence
470 suggests that, despite variation in the $H_{sand,1}$ values, the proportion of Fe^0 in the reactive layer
471 is of paramount significance for system sustainability.
472 Used originally as a model pollutant, methylene blue has exhibited the characteristic of an
473 'operational tracer' or a true indicator. This study has demonstrated that there is much more
474 uncertainty about data collection and their interpretation for the design of Fe^0/H_2O systems
475 than is currently acknowledged. A significant uncertainty arises from the difficulty to assess
476 the time-dependant extent of Fe^0 consumption. An accurate evaluation of the extent of Fe^0
477 consumption would facilitate the prediction of long-term efficiency of Fe^0/H_2O systems.
478 Accordingly, characterization efforts need to be coordinated. Based on the results of the
479 present work, it is suggested that 100 g Fe^0 making about 40 % (v/v) of reactive layers is
480 routinely used in laboratory columns (corresponding H_{rz} about 13 cm for 2.6 cm ID). Ideally
481 each experiment testing porous additives should be accompanied by a reference system where
482 tested Fe^0 is admixed to quartz.

483 **4.8.2 Promoting Fe^0 filtration systems**

484 The results of this work lead to an avenue for reducing uncertainties in designing Fe^0-based
485 filtration systems. Volumetric Fe^0 ratios ensuring long-term efficiency are lower than 50 %.
486 This conclusion determines a 20 years lasting discussion on the suitability and the efficiency
487 of admixing Fe^0 with other materials (e.g. anthracite, gravel, pumice, sand).
488 These results further demonstrated that contaminants should be characterized and tested
489 according to their physical and chemical properties and particularly, their affinity to the

490 Fe^0/H_2O system or to iron corrosion products. The current approach of testing contaminants
491 by their origin (e.g. agricultural wastes (fertilizers and pesticides), heavy metals, human
492 wastes, industrial wastes, organic dyes, pharmaceuticals or radionuclides) is confusing [51].
493 For example, dyes are not an homogeneous class of substances as some of them contain the
494 hydroxyl group (e.g. erichrome black T, bromocresol green, bromophenol blue, fluorescein)
495 and some other (methyl orange, methyl red, and methylene blue) not [54]. With regard to
496 interactions in Fe^0/H_2O systems, dyes with hydroxyl groups exhibit a greater affinity to iron
497 corrosion products. Accordingly, duplicating the experiments reported herein with fluorescein
498 or bromophenol blue as model pollutant will result in longer experimental duration.
499 The results reported herein will enable/facilitate a science-based design of Fe^0-based filtration
500 systems. Based on the observation herein and the theory of the system established before [34],
501 many reported discrepancies can be elucidated. In particular, it is unambiguously established
502 that pure Fe^0 systems are not sustainable. Accordingly, the recent article by Ruhl et al. [24]
503 questioning the theory of the Fe^0-based filters, validated herein, should be regarded as a
504 classical case, illustrating the inefficiency of the data-based approach of developing a theory.
505 This long history of mainstream science teaches that this approach can not be successful [55].
506 Ruhl et al. [24] have recently depreciated the theory of Fe^0-based filters to an assumption and
507 presented data seemingly challenging this theory. They tested anthracite (porous), gravel
508 (compact), pumice (porous) and sand (compact) in dual granular mixtures with a commercial
509 Fe^0 (100 g) in long term column experiments (> 200 days) for the treatment of a
510 trichloroethylene (TCE) contaminated groundwater. Their results confirmed differences in
511 porosity for the tested materials but no difference in 'reactivity' as derived from H_2 evolution.
512 Due to increased cis-dichloroethylene (a TCE metabolite) concentrations in the effluent from
513 all columns (TCE was completely removed), they concluded that "the mixed reactive filters
514 are therefore not applicable for treatment of the here tested groundwater with its indigenous
515 microorganisms". However, this conclusion disproved the results of O'Hannesin and Gillham

516 [1] who have demonstrated the suitability of Fe^0 for contaminant removal at a site
517 contaminated with TCE and PCE (tetrachloroethylene) using a Fe^0:sand weight mixture of
518 22:78.
519 The work presented in ref. [24] shows clearly how misconceptions could be propagated based
520 on wrong interpretation of good experimental observations. To accurately interpret their
521 results, the authors would have additionally tested reference systems (e.g. pure anthracite, Fe^0,
522 gravel, pumice and sand). The results presented herein clearly demonstrated that for short
523 experiments, an inert material could be more efficient than a reactive one. This result
524 confirms that there are no generally efficient or non efficient materials but selected materials
525 should be used to meet the site-specific requirements. In other words, there are appropriate
526 and non appropriate materials. The present work hopes to have opened new avenues to
527 optimised the appropriateness of Fe^0 materials in packed filtration beds, whether they are used
528 for groundwater remediation, wastewater treatment or save drinking water provision.

529 **5 Concluding remarks**

530 This study clearly demonstrates that a pure Fe^0 (100 % Fe^0) filtration system for water
531 treatment is not sustainable. Moreover, even the commonly used 50 % weight ratio is
532 demonstrated not to be the most efficient one. Accordingly, Fe^0 filtration systems must
533 contain less than 50 % (w/w) Fe^0 to be sustainable. The presented work has also validated the
534 suitability of using limited amount of Fe^0 (here 100 g) to investigate relevant processes within
535 reasonable experimental duration (here 4 months) [50]. The rationale for the selection of the
536 admixing materials (e.g. activated carbon, biomaterials, charcoal, gravel, MnO_2, pumice,
537 wood gravel, sand) is yet to be realized. Future works under similar conditions, should use
538 lower pumping rates to increase the probability to experimentally observe permeability loss.
539 In fact, the tested pumping rate (0.1 mL min^{-1}) has solely identified a region (30 to 50 vol %
540 Fe^0) of the optimal Fe^0/sand ratio. An interesting case will consist to test gravity flow which is

relevant for household water filters and for small water treatment plants in remote, low-income communities.

This study has further delineated the unsuitability of the expression of “removal capacity” for Fe^0 materials. This expression could only be acceptable if materials are used under similar conditions, have similar intrinsic reactivity and used in the same mass loading.

The last important feature from this study concerns the long-term reactivity of Fe^0/sand systems. This study has shown that upon an initial increased reactivity Fe^0 oxidation experienced a steady state which was able to produce enough scavengers for the quantitative removal of about 0.6 mg/L methylene blue (30 % of 2.0 mg L^{-1}). Designing a Fe^0/H_2O system could be regarded as finding out such a steady state or creating the conditions for such a state with respect to the actual contaminant flux and the nature of the contaminant of interest. For future works more care should be taken while collecting and interpreting experimental data.

Acknowledgments

The draft manuscript was improved by the insightful comments from Thomas Ptak (Geosciences Center - University of Göttingen). Gerhard Max Hundertmark and Mohammad Azizur Rahman from the Geosciences Center (University of Göttingen) are acknowledged for technical support. The manuscript was improved by the insightful comments of anonymous reviewers from Chemical Engineering Journal.

References

[1] S.F. O´Hannesin, R.W. Gillham, Long-term performance of an in situ "iron wall" for remediation of VOCs, Ground Water 36 (1998) 164–170.

[2] G. Bartzas, K. Komnitsas, Solid phase studies and geochemical modelling of low-cost permeable reactive barriers, J. Hazard. Mater. 183 (2010) 301–308.

566 [3] L. Li, C.H. Benson, Evaluation of five strategies to limit the impact of fouling in
567 permeable reactive barriers, J. Hazard. Mater. 181 (2010) 170–180.
568 [4] S. Comba, A. Di Molfetta, R. Sethi, A Comparison between field applications of nano-,
569 micro-, and millimetric zero-valent iron for the remediation of contaminated aquifers,
570 Water Air Soil Pollut. 215 (2011) 595–607.
571 [5] M. Gheju, Hexavalent chromium reduction with zero-valent iron (ZVI) in aquatic systems,
572 Water Air Soil Pollut. 222 (2011) 103–148.
573 [6] ITRC (Interstate Technology & Regulatory Council) Permeable Reactive Barrier:
574 Technology Update. PRB-5. Washington, D.C.: Interstate Technology & Regulatory
575 Council, PRB: Technology Update Team. www.itrcweb.org (2011).
576 [7] A. Hussam, Contending with a development disaster: SONO filters remove arsenic from
577 well water in Bangladesh, Innovations 4 (2009) 89–102.
578 [8] C. Noubactep, Metallic iron for safe drinking water worldwide, Chem. Eng. J. 165 (2010)
579 740–749.
580 [9] D.E. Giles, M. Mohapatra, T.B. Issa, S. Anand, P. Singh, Iron and aluminium based
581 adsorption strategies for removing arsenic from water, J. Environ. Manage. 92 (2011)
582 3011–3022.
583 [10] L. Li, C.H. Benson, E.M. Lawson, Modeling porosity reductions caused by mineral
584 fouling in continuous-wall permeable reactive barriers, J. Contam. Hydrol. 83 (2006)
585 89–121.
586 [11] S. Roy, P. Bose, Modeling arsenite adsorption on rusting metallic iron, J. Environ. Eng.
587 136 (2010) 405–411.
588 [12] S.-W. Jeen, R.W. Gillham, A. Przepiora, Predictions of long-term performance of
589 granular iron permeable reactive barriers: Field-scale evaluation, J. Contam. Hydrol. 123
590 (2011) 50–64.

591 [13] S.-W. Jeen, R.T. Amos, D.W. Blowes, Modeling gas formation and mineral precipitation
592 in a granular iron column, Environ. Sci. Technol. 46 (2012) 6742–6749.
593 [14] P.D. Mackenzie, D.P. Horney, T.M. Sivavec, Mineral precipitation and porosity losses in
594 granular iron columns, J. Hazard. Mater. 68 (1999) 1–17.
595 [15] P. Westerhoff, J. James, Nitrate removal in zero-valent iron packed columns, Wat. Res.
596 37 (2003) 1818–1830.
597 [16] O.X. Leupin, S.J. Hug, Oxidation and removal of arsenic (III) from aerated groundwater
598 by filtration through sand and zero-valent iron, Wat. Res. 39 (2005) 1729–740.
599 [17] E. Bi, J.F. Devlin, B. Huang, Effects of mixing granular iron with sand on the kinetics of
600 trichloroethylene reduction, Ground Water Monit. Remed. 29 (2009) 56–62.
601 [18] A.M. Gottinger, Chemical-free arsenic removal from potable water with a ZVI-amended
602 biofilter, Master thesis, University of Regina (Saskatchewan, Canada) (2010) 90 pp.
603 [19] N. Moraci, P.S. Calabrò, Heavy metals removal and hydraulic performance in zero-
604 valent iron/pumice permeable reactive barriers, J. Environ. Manag. 91 (2010) 2336–
605 2341.
606 [20] S. Ulsamer, A model to characterize the kinetics of dechlorination of tetrachloroethylene
607 and trichloroethylene by a zero valent iron permeable reactive barrier, Master thesis,
608 Worcester Polytechnic Institute (2011) 73 pp.
609 [21] A.D. Henderson, A.H. Demond, Impact of solids formation and gas production on the
610 permeability of ZVI PRBs, J. Environ. Eng. 137 (2011) 689–696.
611 [22] A.S. Ruhl, A. Weber, M. Jekel, Influence of dissolved inorganic carbon and calcium on
612 gas formation and accumulation in iron permeable reactive barriers, J. Contam. Hydrol.
613 142–143 (2012) 22–32.
614 [23] A.S. Ruhl, C. Kotré, U. Gernert, M. Jekel, Identification, quantification and localization
615 of secondary minerals in mixed Fe^0 fixed bed reactors, Chem. Eng. J. 172 (2011) 811–
616 816.

617 [24] A.S. Ruhl, N. Ünal, M. Jekel, Evaluation of two-component Fe(0) fixed bed filters with
618 porous materials for reductive dechlorination, Chem. Eng. J. 209 (2012) 401–406.
619 [25] R. Crane, C. Noubactep, Elemental metals for environmental remediation: learning from
620 hydrometallurgy, Fresenius Environ. Bull. 21 (2012) 1192–1196.
621 [26] M. Stratmann, J. Müller, The mechanism of the oxygen reduction on rust-covered metal
622 substrates, Corros. Sci. 36 (1994) 327–359.
623 [27] F. Togue-Kamga, K.B.D. Btatkeu, C. Noubactep, P. Woafo, Metallic iron for
624 environmental remediation: Back to textbooks, Fresenius Environ. Bull. 21 (2012)
625 1992–1997.
626 [28] J. Farrell, J. Wang, P. O'Day, M. Conklin, Electrochemical and spectroscopic study of
627 arsenate removal from water using zero-valent iron media, Environ. Sci. Technol. 35
628 (2001) 2026–2032.
629 [29] N.B. Pilling, R.E. Bedworth, The oxidation of metals at high temperatures, J. Inst. Metals
630 29 (1923) 529–591.
631 [30] S. Caré, Q.T. Nguyen, V. L'Hostis, Y. Berthaud, Mechanical properties of the rust layer
632 induced by impressed current method in reinforced mortar, Cement Concrete Res. 38
633 (2008) 1079–1091.
634 [31] M. Rossi, O. Vidal, B. Wunder, F. Renard, Influence of time, temperature, confining
635 pressure and fluid content on the experimental compaction of spherical grains,
636 Tectonophysics 441 (2007) 47–65.
637 [32] H. Jia, C. Wang, Adsorption and dechlorination of 2,4-dichlorophenol (2,4-DCP) on a
638 multi-functional organo-smectite templated zero-valent iron composite Original, Chem.
639 Eng. J. 191 (2012) 202–209.
640 [33] K. Miyajima, C. Noubactep, Effects of mixing granular iron with sand on the efficiency
641 of methylene blue discoloration, Chem. Eng. J. 200–202 (2012) 433–438.

642 [34] S. Caré, R. Crane, P.S. Calabro, A. Ghauch, E. Temgoua, C. Noubactep, Modelling the
643 permeability loss of metallic iron water filtration systems, Clean – Soil, Air, Water, doi:
644 10.1002/clen.201200167.
645 [35] G. Mitchell, P. Poole, H.D. Segrove, Adsorption of methylene blue by high-silica sands.
646 Nature 176 (1955) 1025–1026.
647 [36] S.B. Bukallah, M.A. Rauf, S.S. AlAli, Removal of methylene blue from aqueous solution
648 by adsorption on sand, Dyes and Pigments 74 (2007) 85–87.
649 [37] C. Varlikli, V. Bekiari, M. Kus, N. Boduroglu, I. Oner, P. Lianos, G. Lyberatos, S. Icli,
650 Adsorption of dyes on Sahara desert sand, J. Hazard. Mater. 170 (2009) 27–34.
651 [38] M. Cohen, The formation and properties of passive films on iron, Can. J. Chem. 37
652 (1959) 286–291.
653 [39] C. Noubactep, Characterizing the discoloration of methylene blue in Fe^0/H_2O systems, J.
654 Hazard. Mater. 166 (2009) 79–87.
655 [40] N.W. Barker, H.G. Linge, Methylene blue dye adsorption on sulphide minerals -
656 Relevance to surface area measurement, Hydrometallurgy 6 (1981) 311–326.
657 [41] P.G. Tratnyek, T.E. Reilkoff, A. Lemon, M.M. Scherer, B.A. Balko, L.M. Feik, B.
658 Henegar, Visualizing redox chemistry: Probing environmental oxidation-reduction
659 reactions with indicator dyes, Chem. Educator 6 (2001) 172–179.
660 [42] R.L. Frost, Y. Xi, H. He, Synthesis, characterization of palygorskite supported zero-
661 valent iron and its application for methylene blue adsorption, J. Colloid Interface Sci.
662 341 (2010) 153–161.
663 [43] W.B. Fortune, M.G. Mellon, Determination of iron with o-phenanthroline: a
664 spectrophotometric study, Ind. Eng. Chem. Anal. Ed. 10 (1938) 60–64.
665 [44] M.R. Khan, S.I. Mozumder, A. Islam, D.M. Reddy Prasad, M. Mohibul Alam,
666 Methylene blue adsorption onto Water Hyacinth: Batch and column study, Water Air
667 Soil Pollut. 223 (2012) 2943–2953.

668 [45] N.N. Nassar, A. Ringsred, Rapid adsorption of methylene blue from aqueous solutions
669 by goethite nanoadsorbents, Environ. Eng. Sci. 29 (2012) 790–797.
670 [46] C. Noubactep, The fundamental mechanism of aqueous contaminant removal by metallic
671 iron, Water SA 36 (2010) 663–670.
672 [47] Y.N. Vodyanitskii, Iron hydroxides in soils: A review of publications, Eurasian Soil Sci.
673 43 (2010) 1244–1254..
674 [48] C. Noubactep, T. Licha, T.B. Scott, M. Fall, M. Sauter, Exploring the influence of
675 operational parameters on the reactivity of elemental iron materials, J. Hazard. Mater.
676 172 (2009) 943–951.
677 [49] K. Imamura, E. Ikeda, T. Nagayasu, T. Sakiyama, K. Nakanishi, Adsorption behavior of
678 methylene blue and its congeners on a stainless steel surface, J. Colloid Interf. Sci. 245
679 (2002) 50–57.
680 [50] C. Noubactep, S. Caré, Designing laboratory metallic iron columns for better result
681 comparability, J. Hazard. Mater. 189 (2011) 809–813.
682 [51] K. Kümmerer, Emerging contaminants versus micro-pollutants, Clean – Soil, Air, Water
683 39 (2011) 889–890.
684 [52] K. Nödler, T. Licha, K. Bester, M. Sauter, Development of a multi-residue analytical
685 method, based on liquid chromatography–tandem mass spectrometry, for the
686 simultaneous determination of 46 micro-contaminants in aqueous samples, J. Chromat.
687 A 1217 (2010) 6511–6521.
688 [53] O. Hillebrand, K. Nödler, T. Licha, M. Sauter, T. Geyer, Caffeine as an indicator for the
689 quantification of untreated wastewater in karst systems Original. Water Res. 46 (2012)
690 395–402.
691 [54] B. Saha, S. Das, J. Saikia, G. Das, Preferential and enhanced adsorption of different dyes
692 on iron oxide nanoparticles: A comparative study, J. Phys. Chem. C 115 (2011) 8024–
693 8033.

694 [55] S. Brenner, Sequences and consequences, Phil. Trans. R. Soc. B 365 (2010) 207–212.

695

696

Table 1: Parameters of the packed columns. $H_{sand,1}$ is the thickness of sand preceding the reactive layer; H_{rz} is the thickness of the reactive layer and $H_{sand,2}$ is the thickness of sand after the reactive layer. The internal diameter of the column is 2.6 cm, its length 40 cm as given by the manufacturer but the measured length was 44 cm. The effective volume of the column was 230 mL. The volume occupied by 100 g of Fe^0 was used as unit for the mixture of Fe^0 and sand.

Column	**Fe^0**	**Sand**	**Fe^0**	**Sand**	**$H_{sand,1}$**	**H_{rz}**	**$H_{sand,2}$**
	(g)	(g)	(% v/v)	(% w/w)	(cm)	(cm)	(cm)
1	0.0	-	0.0	100	44.0	0.0	0.0
2	100	87	10.0	46.5	10.0	34.0	0.0
3	100	77	20.0	43.5	11.0	20.0	13.0
4	100	66	30.0	40.5	18.0	15.0	11.0
5	100	58	40.0	36.6	19.0	13.0	12.0
6	100	48	50.0	32.5	18.0	11.0	15.0
7	100	29	70.0	22.4	15.0	7.5	21.5
8	100	19	80.0	16.2	13.0	6.5	24.5
9	100	0.0	100.0	0.0	13.0	6.0	25.0
10	200	0.0	100.0	0.0	15.0	12.5	16.5

Table 2: Summary of the results of the column experiments after 132 days. V_T is the total volume of MB solution which has flowed through each column, $Fe_{effluent}$ and $MB_{effluent}$ are the cumulative mass of Fe and MB in the effluent. $MB_{influent}$ is the total mass of MB which has flowed through the columns. $Fe_{effluent}$ (%) is the ratio of dissolved Fe which has escaped from the column relative to the used mass of Fe^0. E (%) and E_s (mg/g) are the MB discoloration efficiencies (see text). H_{cake} is the thickness of the cake at the entrance of the Fe^0-containing layer as measured at the end of the experiments.

Column	**V_T** (L)	**$Fe_{effluent}$** (mg)	**$MB_{effluent}$** (mg)	**$MB_{influent}$** (mg)	**E** (%)	**$Fe_{effluent}$** (%)	**E_s** (mg/g)	**H_{cake}** (cm)
1	37.6	0.00	19.1	68.89	72.3	-	-	-
2	37.8	47.08	36.4	69.34	47.5	0.047	0.218	2.0
3	37.6	4.01	35.5	68.88	48.4	0.004	0.211	3.0
4	37.8	17.82	25.5	69.39	63.3	0.018	0.239	3.0
5	36.5	6.05	26.6	66.96	60.3	0.006	0.192	2.3
6	37.5	8.40	28.6	68.73	58.4	0.008	0.201	1.5
7	37.6	6.96	36.4	68.97	47.2	0.007	0.159	1.3
8	37.5	9.71	40.0	68.74	41.9	0.010	0.143	1.1
9	38.1	7.82	35.8	69.77	48.7	0.008	0.195	1.0
10	37.8	4.91	22.0	69.37	68.3	0.002	0.154	1.0

716 **Table 3**: Correlation parameters of the straight lines $[MB]_{effluent} = a*[MB]_{inffluent} + b$ for the 10
717 columns. “a” is the rate at which MB concentration increases in the effluent after
718 breakthrough. “b” is the point at which each straight line MB meats the $[MB]_{effluent}$-
719 axis. R is the correlation factor and N is the number of experimental points used for
720 the plot. Fig. 4 suggests that the smaller the a values, the more efficient the systems.
721

Fe^0	**N**	**R**	**a**	**δa**	**b**	**δb**
(%,vol)	(-)	(-)	(-)	(-)	(-)	(-)
0	4	0.9881	0.31	0.03	-26.3	3.3
10	14	0.999	0.64	0.01	-14.4	0.4
20	10	0.998	0.63	0.02	-15.3	0.6
30	8	0.997	0.55	0.02	-17.1	0.8
40	8	0.996	0.56	0.02	-16.8	0.9
50	8	0.998	0.60	0.02	-17.8	0.7
70	12	0.999	0.65	0.01	-13.4	0.3
80	12	0.999	0.74	0.01	-14.4	0.3
100	11	0.998	0.65	0.01	-14.6	0.5
100	6	0.999	0.65	0.01	-23.0	0.5

722
723
724

Figure 1

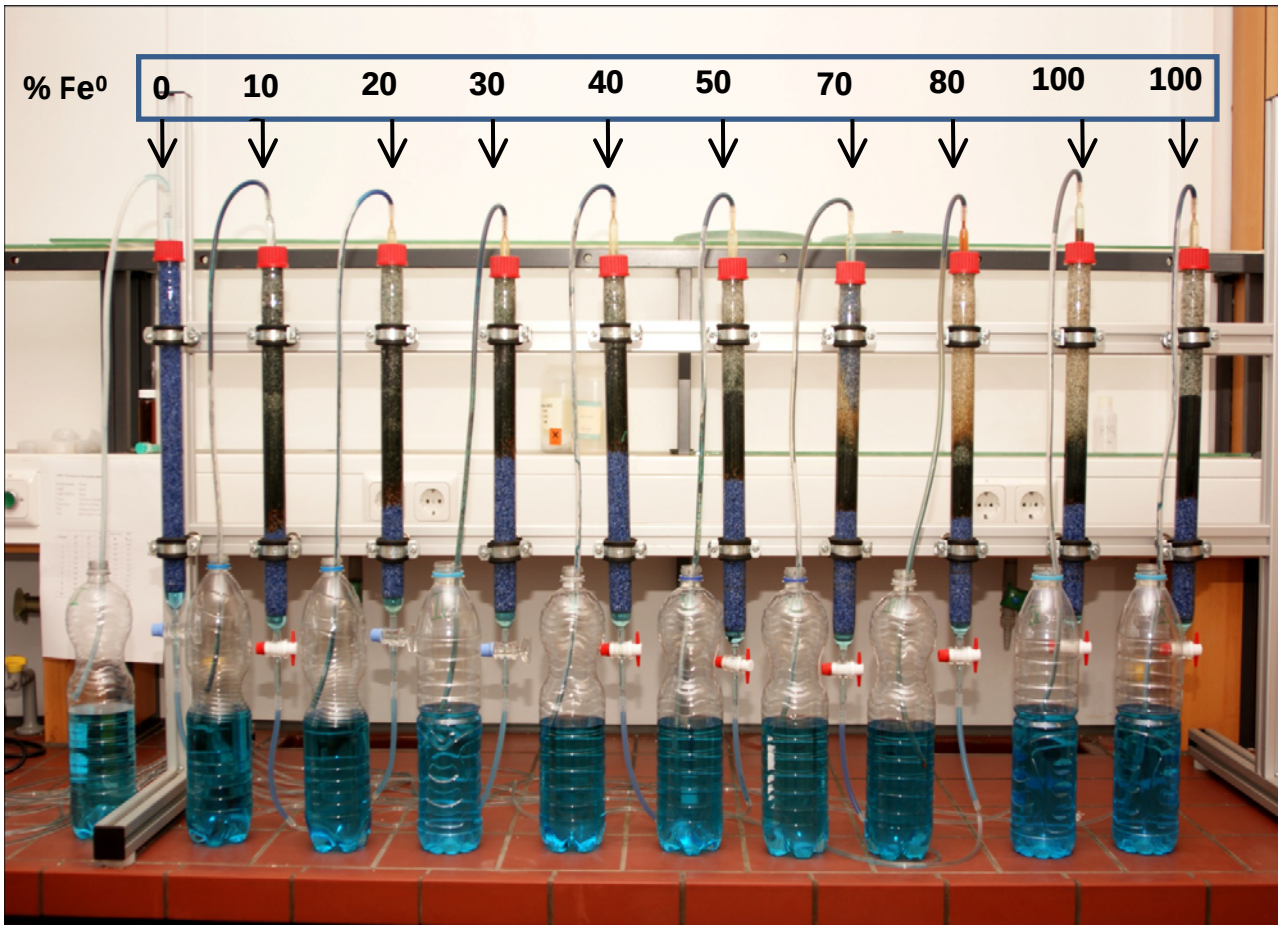

730 **Figure 2**

731

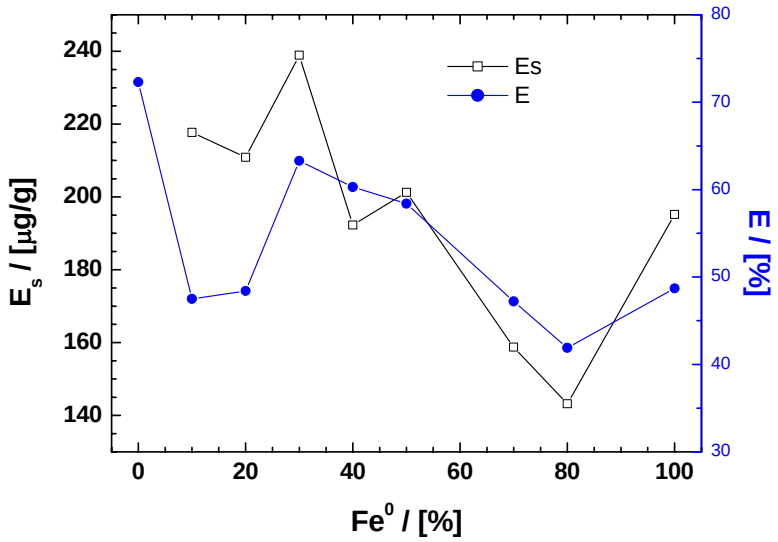

732

733

733 **Figure 3**

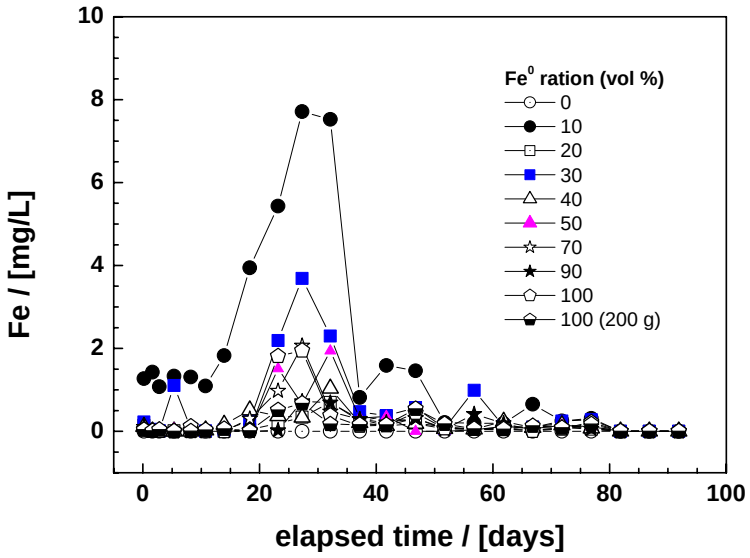

734

735

735 **Figure 4**

736

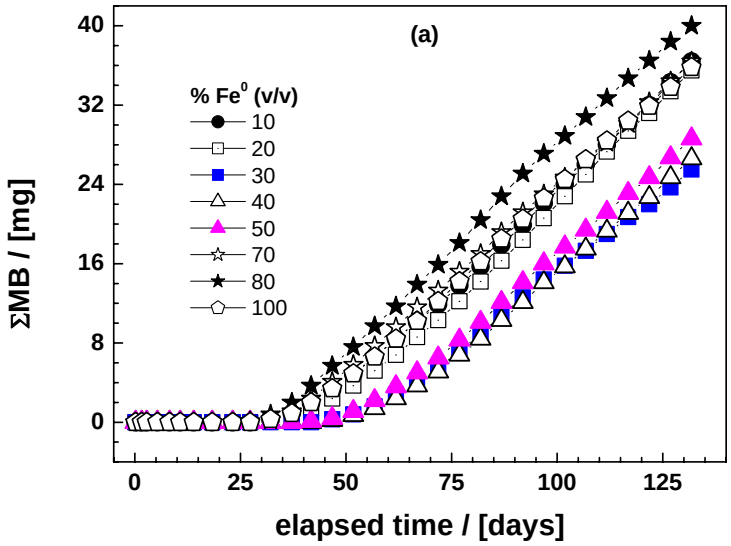

737

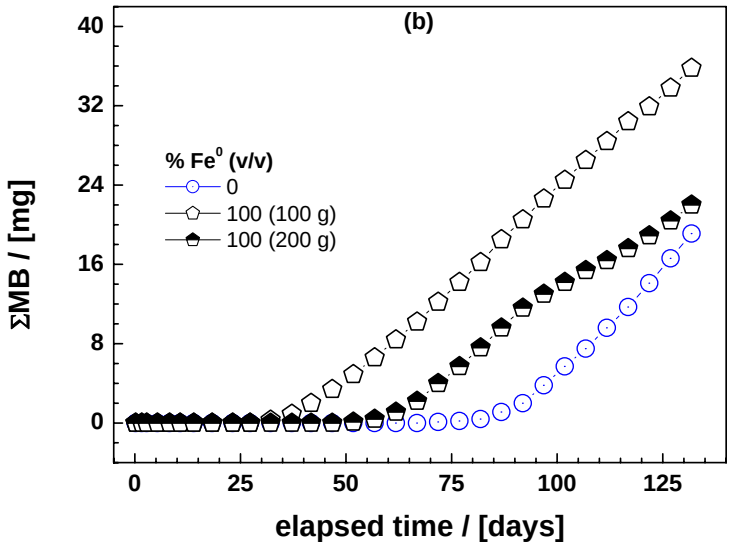

738

739

740

741

742

743

743 **Figure 5**

744

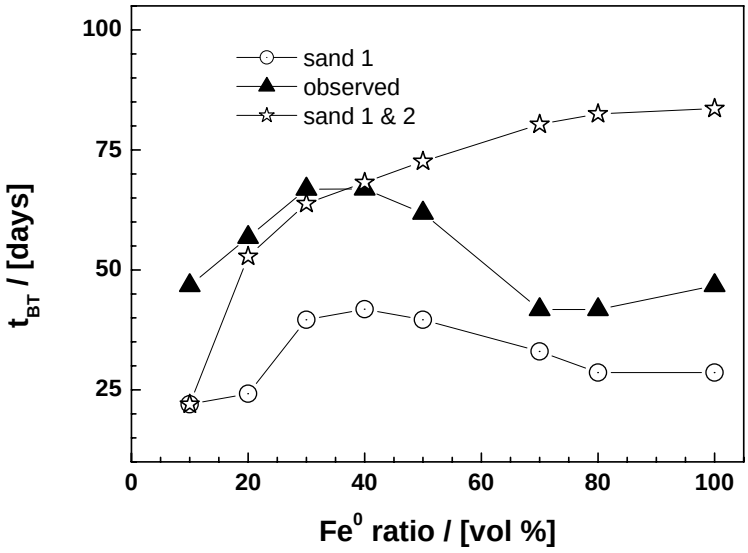

745

746

747

747 **Figure 6**

748

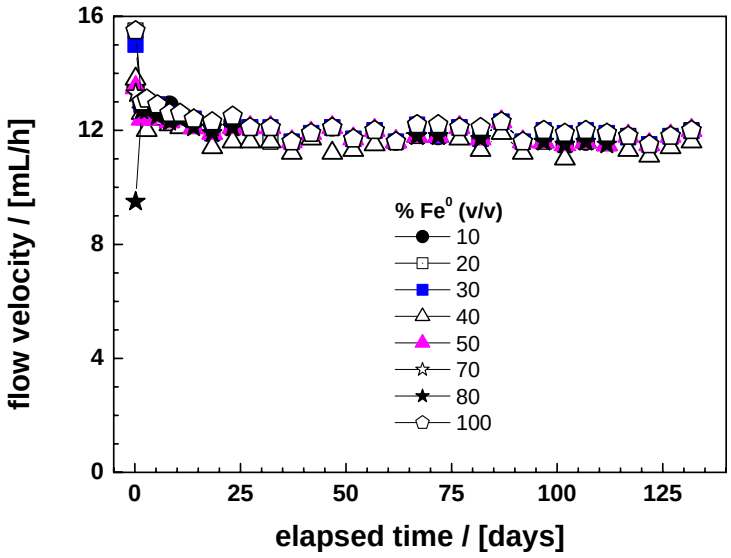

749

750

Figure 7

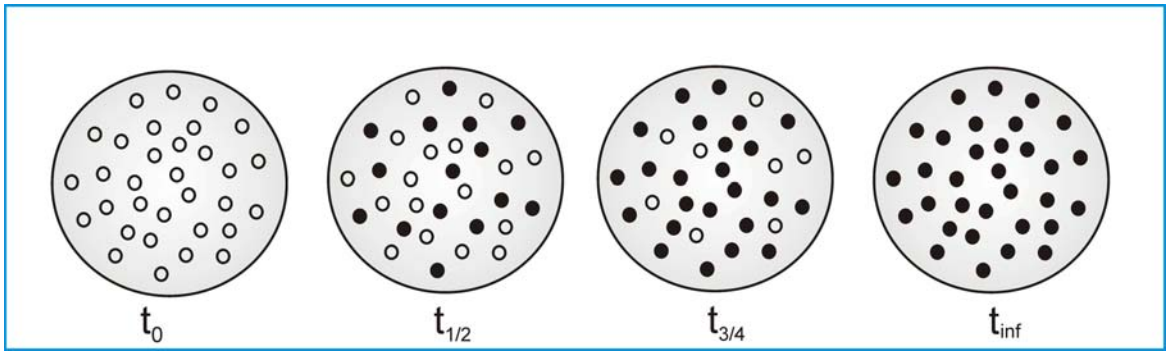

754 **Figure 8**

755

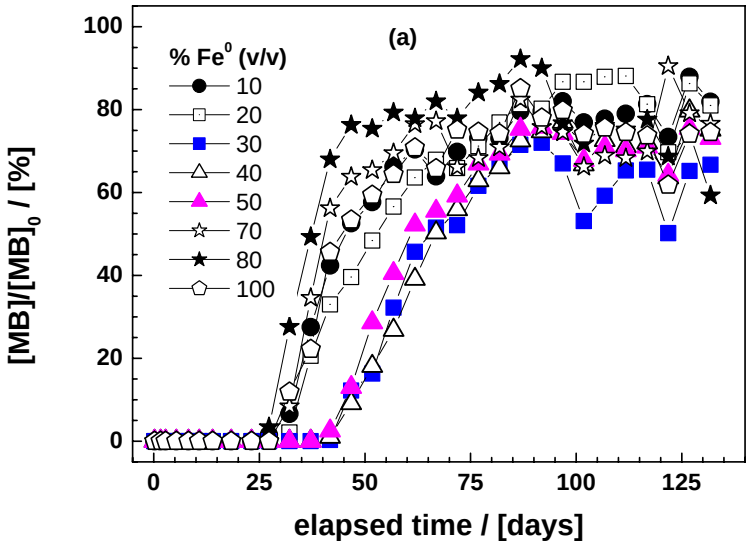

756

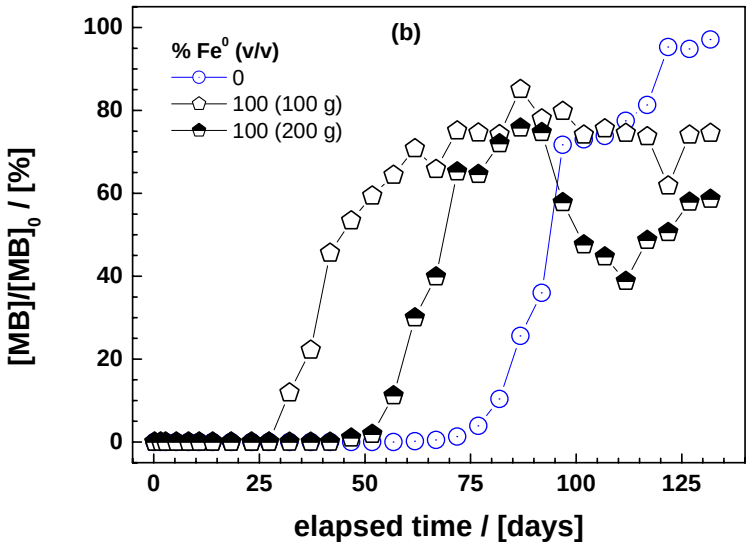

757

758

Figure 9

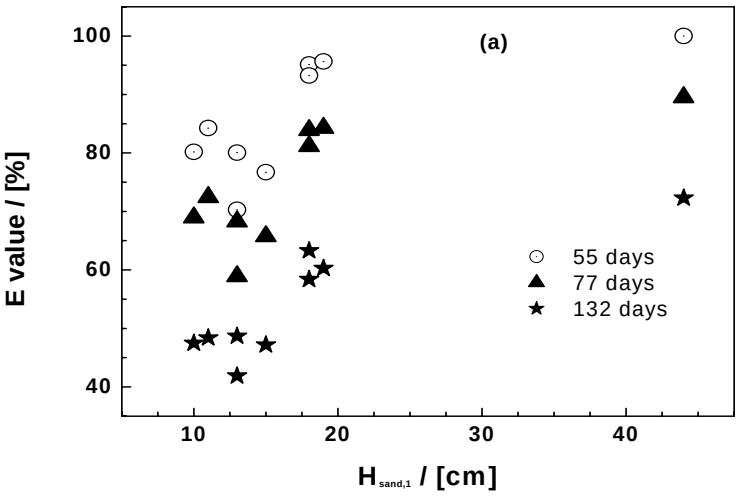
(a)
E value / [%]
100
80
60
40
10
20
30
40
$H_{sand,1}$ / [cm]
55 days
77 days
132 days

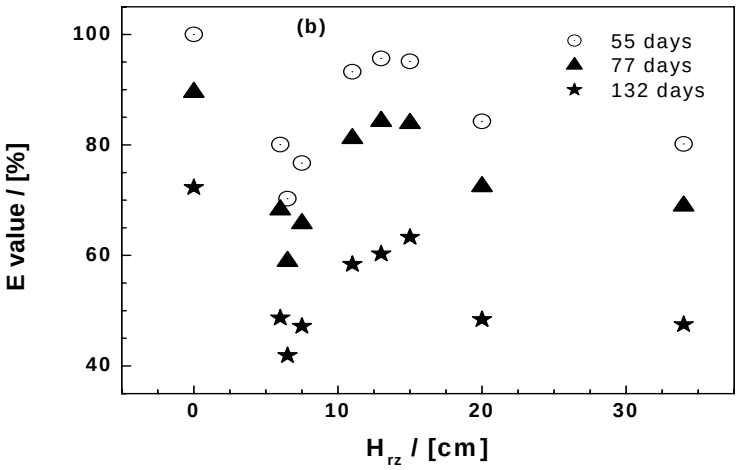
(b)
E value / [%]
100
80
60
40
0
10
20
30
H_{rz} / [cm]
55 days
77 days
132 days

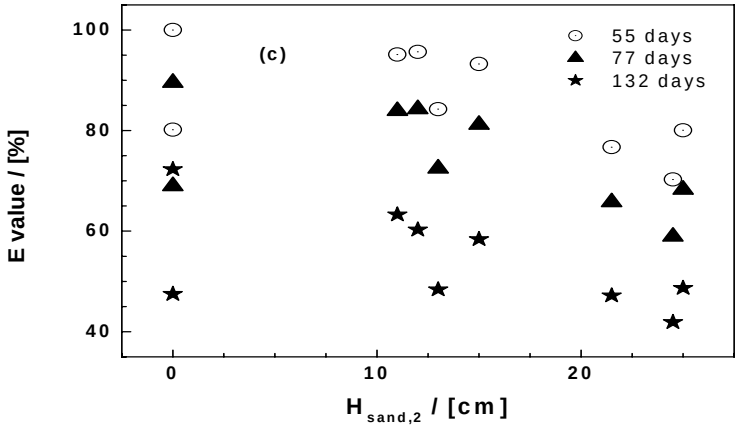
(c)
E value / [%]
100
80
60
40
0
10
20
$H_{sand,2}$ / [cm]
55 days
77 days
132 days

762 **Figure captions**

763

764 **Figure 1:** Photograph of the experimental design, showing the 10 columns at the end of the
765 experiment (day 132). Uniform migration of the MB front is observed before the Fe^0 layer
766 ($H_{sand,1}$ - Tab. 1). MB breakthrough is observed in all systems. The absence of an MB
767 adsorption front beyond the Fe^0 layer evidences the disturbance of the flow regime within this
768 layer.

769

770 **Figure 2**: Effect of Fe^0 amendment on the discoloration (E and E_s) of methylene blue after
771 132 days. The lines are not fitting functions, they simply connect points to facilitate
772 visualization.

773

774 **Figure 3**: Time-dependant evolution of the iron concentration of column effluent. The lines
775 are not fitting functions, they simply connect points to facilitate visualization.

776

777 **Figure 4:** Effect of Fe^0 amendment on the performance of sand column for methylene blue
778 discoloration: (a) 100 g of Fe^0 occupying a volumetric proportion of 10 to 100 % of the
779 reactive zone; and (b) 100 and 200 g of Fe^0 in a pure Fe^0 reactive zone. The lines are not
780 fitting functions, they simply connect points to facilitate visualization.

781

782 **Figure 5:** Comparison of model predictions of MB breakthrough with experimental
783 observations after 97 days. The model assumes uniform MB adsorption onto sand 1 and sand
784 2 (see Table 1). The lines are not fitting functions, they simply connect points to facilitate
785 visualization.

786

Figure 6: Time-dependant evolution of the flow velocity curves in the 8 tested systems. The lines are not fitting functions, they simply connect points to facilitate visualization.

Figure 7: Cross-sectional diagram of the time-dependent evolution of the porosity in a Fe^0/sand cylindrical column in which Fe^0 experiences uniform corrosion. t_0, $t_{1/2}$, $t_{3/4}$ and t_∞ (t_{inf}) are the times at which porosity loss is 0, 50, 75 and 100 % respectively. As a rule the 'filter resistance' increases with increasing porosity loss.

Figure 8: Breakthrough curves of MB discoloration in the 8 tested systems (a) and in the 3 pure material systems (b). The lines are not fitting functions, they simply connect points to facilitate visualization.

Figure 9: Correlation of the cumulative extent of MB discoloration at days 55, 77 and 132 as function of the high of (a) sand before the reactive zone ($H_{sand,1}$), (b) the reactive zone (H_{rz}) and (c) sand after the reactive zone ($H_{sand,2}$). The reference system (0 % Fe^0) corresponds to $H_{sand,1}$ = 44 cm or H_{rz} = $H_{sand,2}$ = 0 cm. For the 10 % Fe^0 system, $H_{sand,2}$ = 0.